Design Concepts for Diffusive Holographic Photopolymers

Benjamin A. Kowalski, Robert R. McLeod

Department of Electrical, Computer, and Energy Engineering, University of Colorado at Boulder, 425 UCB, Boulder, Colorado 80309
Correspondence to: R. R. McLeod (E-mail: robert.mcleod@colorado.edu)

Received 31 August 2015; accepted 18 December 2015; published online 14 March 2016
DOI: 10.1002/polb.24011

ABSTRACT: Diffusive photopolymers are an area of intense recent materials development, spurred by interest in holographic data storage, display holography, and custom diffractive optical elements, among other applications. This review examines a range of photopolymer formulations of academic and commercial interest, and places their design strategies in context via quantitative analysis of the recording fidelity, maximum refractive index change and the degree to which they achieve this limit. Finally, this analysis is extended to estimate the scope of achievable future performance improvements. © 2016 Wiley Periodicals, Inc. J. Polym. Sci., Part B: Polym. Phys. **2016**, *54*, 1021–1035.

KEYWORDS: data storage; diffractive optical elements; holography; optics; photopolymers; photopolymerization; reaction/diffusion kinetics; refractive index

INTRODUCTION Holographic recording media respond to a three-dimensional (3D) optical pattern with a permanent refractive index change approximately proportional to local energy dose. Photopolymer media create this refractive index pattern via polymerization reactions that drive diffusion of an initially homogeneous mixture of two components of contrasting refractive index. This compositional gradient thus creates an index modulation without wet chemical processing, in contrast to other photopolymer patterning techniques that require a solvent wash or developer solution. This self-processing makes holographic photopolymers an appealing material platform for applications which require thick media layers that are not amenable to wet processing.

These include applications in which the index modulations serve either as a recording medium (e.g. data storage, display holography) or as optical elements (e.g. custom GRIN components, integrated optical devices). All these applications are characterized by simultaneous stringent requirements on both optical properties (achievable index modulation, sensitivity) and mechanical and process properties (cheap, rugged, mechanically stable). We show that diffusion-driven photopolymers are particularly well suited to address these requirements, and then survey the literature to quantify the reaction/diffusion kinetics in these materials despite unique metrology challenges.

Finally, we argue that the primary purpose of these materials is to respond to incident intensity with the largest possible refractive index pattern that is a faithful copy of the intensity distribution. The role of the photoactive chemistry is thus to absorb light and create a compositional segregation while satisfying secondary goals such as sensitivity and shrinkage. Since the maximum refractive index change can be calculated as the complete segregation of the mobile species in the formulation, it is a useful metric to quantitatively compare the potential and achieved performance of materials. We show that this "formula limit" on maximum refractive index can be calculated for many significant formulations from the literature, using only data already reported. Trends in the degree to which results approach this limit enable comparisons of different reactive groups, determination of resolution limits and potential for further material improvement independent of confounding variables such as the particular species refractive index or formulated concentrations. Importantly, this calculation does not require a comprehensive reaction/diffusion model of each chemical system since it focuses only on the refractive index arising from the compositional gradients driven by the chosen chemistry.

APPLICATIONS AND DESIGN SPECIFICATIONS

Commercial development of optically driven diffusive photopolymers has been motivated by two classes of applications: first, thick (~1 mm) media layer applications including holographic data storage (HDS); and second, thin film (~20 μm) applications including display and security. These two classes

Additional Supporting Information may be found in the online version of this article.

Dr. Benjamin Kowalski is a postdoctoral researcher at the Air Force Research Lab at Wright-Patterson AFB. His research interests include diffractive optical elements as realized in either liquid crystal elastomers or conventional holographic photopolymers. He holds degrees from the University of Colorado and Kenyon College.

Dr. Robert McLeod is Department Chair and the Richard and Joy Dorf Endowed Professor of Electrical, Computer and Energy Engineering at the University of Colorado Boulder and a topical editor for Optics Letters. His research group specializes in the interaction of light and organic materials with applications to lithography, integrated optics, computational imaging and cellular biology. He holds graduate degrees from Montana State University, University of California, and the University of Colorado.

will be considered in turn, as they have somewhat different performance specifications.

First, HDS exploits volumetric rather than surface patterning, and thus thick media layers are essential to achieve high storage densities and throughputs.[1] This concept can be realized through various parallel transfer (or "page-based") architectures[2] or through serial transfer (or "microholographic") approaches.[3] In all cases, the achievable performance (i.e. storage density and transfer rate) depends, via the Shannon limit, on the available refractive index modulation Δn, the available spatial frequency bandwidth (i.e. media spatial resolution), and noise caused by optical scatter. Increased Δn yields monotonic gains in performance, with a scaling that depends on the specific storage architecture.[4,5] However, this increased Δn generally also incurs greater penalties in recording-induced shrinkage and optical scatter, leading to a highly constrained materials design problem in which noise and distortion must be traded off against fast recording and high diffraction efficiency.

Other thick-layer applications include diffractive optical elements (DOEs), either single-layer or stratified, which find applications in shear interferometry,[6] spatial filtering (either external[7] or intracavity[8]), and signal processing (e.g. optical correlators[9]). Low-cost, customizable recording of arbitrary DOEs, as has been demonstrated in photopolymers,[10] is of interest for endoscopic probes, contact lenses and intraocular lenses (including UV recording of custom index profiles *in vivo* after implantation[11]).

Finally, thick media layers also enable integrated optical devices, recorded either via a focused, rastered beam,[12] via mask exposure,[13] or via self-writted waveguides.[14] Here, instead of painstaking mechanical alignment of individual optical components, the components are encased in a monolithic layer of photopolymer, and then waveguides are drawn through the monolith to connect them.[15] These waveguides, in conjunction with other recorded components including couplers,[16] optical interconnects,[17] and coherent waveguide arrays,[18] together enable the realization of complete integrated devices. Even greater functionality is enabled by Bragg gratings, which can serve as filters for wavelength multiplexing,[19] as resonators for polymer lasers,[20] as mechanical sensors, or as chemical sensors for applications including vapor detection[21] and tear glucose monitoring in contact lenses.[22] These can be further integrated with microfluidics within a single material platform for lab-on-a-chip applications.[23]

Next we turn from thick media layers to thin-film applications, including diffusers for LED backlighting,[24] transparent heads-up displays,[25] concentrators for solar panels,[26] printed display holograms[27] and security holograms.[28] These applications demand high index modulations, on the order $\Delta n \sim 0.05$, in order to achieve wavelength-scale optical path differences through a media layer of only $\sim$20 μm. Conversely, the tolerances on recording-induced shrinkage and optical scatter are relaxed for such thin layers (and further relaxed in reflection geometries, given the typical angular distribution of scatter). Spatial resolution requirements are stringent, however, since the reflection hologram geometry corresponds to fringe spacing of approximately $\lambda/3$. Finally, the media must be sufficiently rugged to withstand challenging environmental conditions, including abrasion or ultraviolet exposure from sunlight.

For all of these applications, three performance specifications are crucial: dynamic range (Δn), sensitivity, and passive optical properties. We consider each in turn.

The dynamic range, i.e. total achievable refractive index modulation Δn, is of primary importance since it is directly related to the desired performance. This material property is sometimes instead reported in terms of the corresponding system property, $M_{\#}$ that simplifies to $\pi \Delta n L/(\lambda \cos\theta)$ for

plane waves.[29] For integrated optical components, Δn determines key performance specifications such as the achievable optical power of a gradient-index lens, or the mode size of a waveguide. For display holograms, Δn determines the achievable diffraction efficiency at a particular layer thickness. Likewise, for holographic data storage, Δn determines the number of holograms M of a given diffraction efficiency $\eta = \left(M_{\#}/M\right)^2$ that can be recorded in a given volume of media, and therefore the achievable storage density and transfer rate.

The secondary specification is typically high sensitivity (i.e. Δn produced by a specified exposure dose in mJ/cm^2), especially for commercial applications that require high throughput using inexpensive, low-power lasers. This specification may also include the requirement of linearity in index response with respect to both exposure dose and irradiance (in mW/cm^2). Any sublinearity in response, such as that arising from bimolecular termination,[30] implies a loss in recording fidelity and therefore wasted dynamic range.

Next, the sensitivity should be high and nearly uniform at the desired spatial frequencies, and—ideally—weaker at undesired spatial frequencies associated with e.g. noise written by optical scatter,[31] or optical aberrations written by the macroscopic beam profile.[5,32] Diffusive photopolymers, for example, typically have a high spatial frequency cutoff due to diffusional blurring, as well as a low spatial frequency cutoff due to limited long-range diffusion caused by vitrification or finite time to post-exposure flood curing.

This sensitivity is typically specified to be at a desired optical wavelength or wavelengths. Data storage applications are practically limited to laser diode sources, and thus the recording wavelength can currently be no lower than ~405 nm. Display holography applications use multiple initiators in order to achieve good sensitivity spanning the visible spectrum; initiators at longer wavelengths typically also require an electron donor or other sensitizer.[33]

Consumption of photoinitiator leads to an unwanted decrease in sensitivity with dose. This effect can be compensated by scheduling of successive exposes[34] or dynamic modulation of a rastered writing focus,[35] or it can be mitigated by using a high photoinitiator concentration, while at the same time ensuring that the recording wavelength is sufficiently far onto a low-absorptivity shoulder that the overall Beer-Lambert absorption is still tolerably low for a given media thickness.

Finally, in addition to the active (recording-induced) optical properties discussed so far, the passive/bulk optical properties must also be considered, especially for thick media layers. These include optical clarity (i.e. low intrinsic scatter), transparency, and phase uniformity.

In photopolymers, two general strategies exist for achieving these passive optical specs: "single-chemistry" or "two-chemistry." In the single-chemistry strategy, the system comprises a monomer, photoinitiator, and high molecular weight binder. The same photopolymerization chemistry is used both to record patterned features and to crosslink the entire media layer. Typically this crosslinking is achieved through a partial, uniform optical cure before and/or after the patterned recording exposure (e.g. Refs. 36 and 37).

In the two-chemistry strategy, first a solid host matrix is formed (typically thermoset, or possibly thermoplastic[38]), and then a second, orthogonal chemistry is used to initiate (typically radical) photopolymerization. This two-chemistry approach is increasingly preferred in commercial holographic media[34] due to its additional design freedoms: the matrix polymer that dominates passive properties (e.g. modulus and phase flatness) can be engineered independently from the writing polymer that dominates the recording properties (e.g. index contrast and scatter). This additional design freedom enables better passive optical properties, particularly when the matrix thermally cures via a step-growth process.

The volume fraction of the media dedicated to recording properties such as Δn (i.e. the writing chemistry) must be carefully balanced against the fraction dedicated to passive properties (i.e. the matrix). This tradeoff becomes particularly significant as the writing chemistry fraction is increased enough to achieve high Δn (>0.01) as will be shown below. This will be the first in a series of intrinsic tradeoffs between opposing requirements that are characteristic of the design of two-chemistry media.

Along with these optical requirements, there are also stringent mechanical specifications. Thick (i.e. Bragg regime) holographic elements are extraordinarily sensitive to polymerization-induced volume shrinkage. Not only does this shrinkage distort the holographic fringes, but, it is typically anisotropic via the Poisson ratio due to the mechanical constraints imposed by the packaging of the media layer. Because of this anisotropy, shrinkage can only partially be compensated by tuning the readout angle (or wavelength, as in Ref. 34). Thus, tolerances on recording-induced volume shrinkage can be as stringent as 0.05% for typical holographic data storage architectures, imposing additional constraints on the volume fraction that can be dedicated to the writing chemistry.

Similarly, thick holographic elements are highly sensitive to thermal expansion. This leads to another design tradeoff: a high glass transition temperature T_G of the matrix is associated with a favorably low coefficient of thermal expansion (CTE). But, conversely, a low T_G enables fast diffusive recording, and is also associated with lower matrix refractive index and thus greater index contrast.[39] Even formulations approaching the high-T_G limit of this tradeoff, with $T_G \sim 26$ °C, still exhibit a CTE as large as 500 ppm per °C, enough to significantly restrict the operating temperature range.[40]

Finally, other mechanical properties such as elastic modulus and scratch hardness become important in cases where media must be exposed directly to the environment without

protective packaging, as is especially common for integrated optical devices. This poses another, similar design tradeoff: high matrix T_G is associated with good mechanical ruggedness,[41] but low T_G is favorable for diffusive recording as discussed above. This tradeoff can be circumvented in recently developed two-stage systems in which a low-T_G recording step is followed by a matrix hardening step.[41]

Finally, in addition to these optical and mechanical specifications, commercial media must satisfy a set of process requirements. Most notably, media must be produced at low cost in the desired form factor up to millimeter thickness. This is typically achieved with a thermosetting polymer, whether mold-cast for thick layers, or roll- or spun-cast for thin films. The media must then remain stable for some shelf life prior to exposure. For polymerization-based writing chemistries, this may require the addition of inhibiting species (or ambient oxygen may be sufficient to inhibit radical processes). After exposure, the recorded features must remain stable for as long as decades (in the case of data storage), in the presence of humidity, heat, and ambient light including both UV and long-wave radiation. Other stability concerns include delamination, yellowing, and out-diffusion of volatile organic compounds.

Despite the intrinsic design tradeoffs enumerated above, diffusive photopolymers compare favorably to other material platforms, as will be discussed in the following section.

OTHER CANDIDATE MATERIAL PLATFORMS

First we consider index modulation mechanisms that are not driven by mass transport. These have the advantage that they can readily be implemented in a glassy host matrix, which affords good optical clarity, bulk mechanical ruggedness, and negligible volume shrinkage.

Multiphoton absorption in glass (typically fused silica) can generate permanent structural changes, through localized melting or even microvoid formation.[42] The same technique can be applied to glassy polymers such as poly(methyl methacrylate).[43] Because multiphoton absorption cross-sections are characteristically very low, this mechanism has low sensitivity and thus requires a pulsed, focused writing beam. The writing beam can be raster-scanned to record sparse waveguide structures[44] or volume computer-generated holographic elements,[45] but cannot achieve high-throughput recording due to the low sensitivity.

Another refractive-index forming mechanism is the photorefractive effect, in which diffusion of electrons induces an index structure via the subsequent space charge field. Photorefractive polymers[46] are easily fabricated by casting or by spinning from liquid precursors, in contrast to photorefractive crystals that require an expensive process of crystal growth, cutting, and polishing.[47] The dynamic range of these polymer media is typically low ($\Delta n \sim 3 \times 10^{-4}$), but can be greatly enhanced by using polar chromophores that are reoriented by a strong applied electric field.[48] Unlike the inherently permanent structures recorded by photopolymers, refractive index gratings in photorefractive polymers can typically be optically erased and thermally relax in the absence of the poling field. These media also suffer from the characteristically low sensitivity of two-photon mechanisms, order 10^{-6} cm^2/J.

Therefore we turn next to mechanisms driven by single-photon absorption, such as photochromism, Here, a glassy host matrix such as PMMA is doped with a photochromic dye, traditionally an azo dye,[49] although ortho-nitrostilbene[50] and Dewar benzene derivatives[51] are among others that have been explored. Again, bulk optical properties are good, and recording does not induce significant volume shrinkage. Thermal stability is poor, as is the dynamic range ($\Delta n \sim 3 \times 10^{-5}$), but both of these can be improved via the addition of mesogenic side groups, which stabilize the reorientation and give resonance enhancement to the index change,[52] up to a remarkable $\Delta n \sim 0.5$.

Finally, chalcogenide glasses exhibit a complex and incompletely understood range of photoinduced effects, including photodarkening due to changes in bond structure,[53] photorefractive effects, changes from amorphous to crystalline phase, and dissolution of metals followed by mass transport.[54] Photoinduced structural changes can yield a dynamic range of up to order 0.1, with fair sensitivity, of order 0.1 cm^2/J.[55]

Next we consider index modulation via mass-transport-driven compositional modulation. This mechanism affords not only high sensitivity and dynamic range, but also the ability to permanently "fix" recorded features with a final optical cure that renders the media insensitive to further exposure. However, this mechanism also poses new challenges in meeting the mechanical, bulk optical, and process specifications. Dichromated gelatins, for example, achieve a dynamic range as high as $\Delta n \sim 0.1$ due to the formation of air-filled microvoids.[56] However, they have limited sensitivity and high recording-induced shrinkage, and require cumbersome wet chemical processing. The historically important silver halide gelatins[57] boast a comparably high dynamic range along with sensitivity as high as order 100 cm^2/J, but also suffer from the need for wet processing.

Another approach, suitable for implementation in glassy host matrices, relies on the mass transport of chromophores. Upon photo-exposure, an initially mobile chromophore is selectively attached to the matrix, as in the classic PQ/PMMA system[58] or the more recent NQ/PMMA;[59] or else an initially attached chromophore is selectively released.[60] Diffusion through the glassy matrix is normally negligibly slow, but a post-baking step speeds it up dramatically, so that the mobile chromophores diffuse to equilibrium, thereby generating a moderately strong index modulation. It should be emphasized that each photon absorption event produces at most a single bond-forming or -breaking event; in other words, there is no chemical amplification. This leads to low shrinkage, as compared to radical photopolymerization,

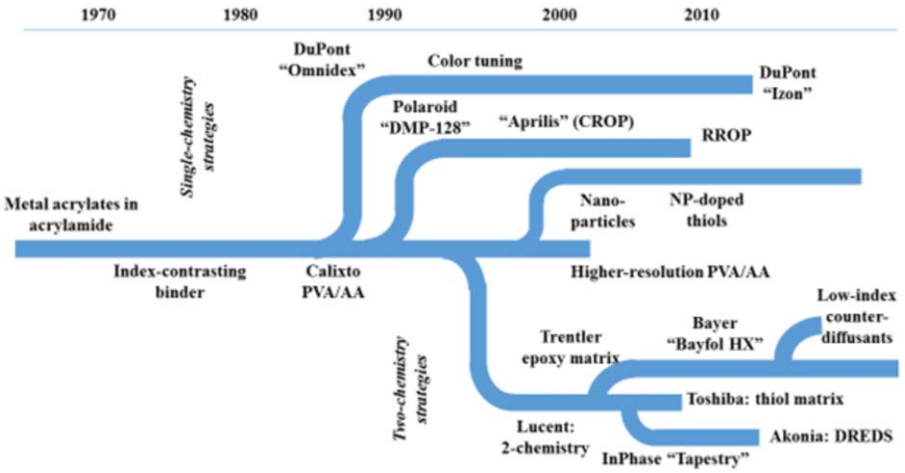

FIGURE 1 An evolutionary tree of holographic photopolymer formulations of particular academic or commercial significance, illustrating two general design strategies: single-chemistry and two-chemistry. A more quantitative survey of these same formulations follows below.

which forms long polymer chains with fewer degrees of freedom.

However, these systems with no chemical amplification achieve only moderate sensitivities, of order $\sim$0.1 cm^2/J. Amplified mechanisms such as chain growth, in which a single photon-absorption event initiates a long chain of polymerization events, achieve sensitivities as high as order 10 cm^2/J routinely, satisfying the demands of high-throughput commercial applications. These materials can also satisfy the other optical, mechanical, and process requirements discussed above, including Δn as high as $\sim$0.05, although their chemical composition must be carefully tuned to balance these various requirements. In the next section we consider these material design problems in more detail.

DESIGN OF DIFFUSIVE PHOTOPOLYMERS

Binder or Matrix

As shown in Figure 1, materials development of holographic photopolymers falls into the two overarching design strategies discussed above. The single-chemistry strategy, using a high-molecular-weight binder, is utilized in several commercially important media. DuPont's Omnidex films use high-index acrylate writing monomers and cellulose-based binders; they achieve good dynamic range ($\Delta n \sim 0.06$) upon thermal post-processing to facilitate diffusion.[61] Polaroid's DMP-128 films use acrylate writing monomers and a polyethylene imine binder. Subsequent solvent processing leads to the formation of micropores in the exposed regions.[62] Since the pores are filled with air or with some highly index-contrasting solvent,[63] the resulting index modulation can be quite high, $\Delta n \sim 0.08$, with good sensitivity, $\sim$5 cm^2/J.

The two-chemistry strategy, in which the binder is replaced by a thermoset crosslinked host matrix, was first demonstrated commercially by Lucent spinoff InPhase. The InPhase media used only enough writing chemistry to achieve a modest $\Delta n \sim 3 \times 10^{-3}$ (with sensitivity of 4.5×10^{-3} cm^2/J), and thus could be cast in mm-thick layers while still maintaining excellent scatter and shrinkage properties. Bayer's Bayfol HX media, conversely, targeted thin ($\sim$20 μm) film applications, which demand higher Δn but can tolerate greater recording-induced scatter and volume shrinkage. Thus, a greater concentration of writing chemistry was used, enabling a higher $\Delta n \sim 0.04$ (with $\sim$2 cm^2/J sensitivity).[64] Most recently, InPhase's successor Akonia has utilized the "DRED" technique to reduce the wasted fraction of the consumed writing chemistry, leading to a dramatically improved $\Delta n \sim 0.05$.[65]

Alternatively, this polymer host matrix can be replaced by nanoporous glass, into which a photopolymer resin is infiltrated. The glass has excellent bulk mechanical rigidity and negligible volume shrinkage, and yet still affords fast diffusion through the network of pores.[66] Fabrication of nanoporous glass remains prohibitively expensive, but a promising alternative is hybrid inorganic-organic sol-gel glasses.[67]

Photoinitiator

Radical polymerization is a common choice for writing chemistry, in part because of the availability a large toolbox of well-understood photoinitiators. One notable exception, cationic ring-opening polymerization initiated by e.g. iodonium salts, will be discussed in the subsequent section.

Of more recent interest are macro-photoinitiators, which are slower to undergo unwanted diffusion into unexposed regions, and can even be fully tethered to the matrix.[68] Additionally, macro-photoinitiators can be less susceptible to cage recombination reactions, which often produce unwanted volatile organic photoproducts.[69]

Another area of recent interest is two-photon initiation, which affords a sharp reduction in unwanted out-of-focus

material response. Two-photon absorption cross-sections are so small that the required intensities can only be achieved via a focused (and often pulsed) rastered writing beam, leading to severe constraints on achievable throughput. Although the two-photon cross-sections of many standard photoinitiators have been well characterized,[70] little attempt has been made to model the subsequent reaction/diffusion kinetics. Furthermore, since the two-photon initiation pathway cannot be used for a large-area postcure, current realizations of two-photon recording simply allow a significant amount of unconsumed, volatile monomer and photoinitiator to remain present in the media after recording.[71]

Writing Monomer

The volume fraction of writing monomer must be carefully tuned to balance two opposing requirements.[72] A higher concentration of monomer will increase the index modulation of recorded features (the "signal" term) but will also increase recording-induced optical scatter (often the dominant "noise" term). Making matters worse, it will also increase the recording-induced volume shrinkage, which leads to distortion of recorded features, especially in thick samples.

Thus, design of a media with good "signal-to-noise" recording performance is guided by two general considerations: first, maximizing the index-contrast benefit achieved per bond converted, and second, minimizing the shrinkage and scatter penalties accrued per bond converted.

To maximize the index-contrast benefit per bond converted, it is advantageous to synthesize monomers containing a large number of index-contrasting groups per reactive group. Since the matrix is often chosen to be low index, consistent with low T_G, these index-contrasting groups are then typically high-index aromatic groups or heavy atoms. Taking this approach to its extreme, highly dendronized macromonomers have been shown to reduce volume shrinkage to as low as 0.04% while maintaining a moderate index contrast of $\Delta n \sim 2 \times 10^{-3}$.[73] Further increases in macromonomer size are ultimately limited by solubility in the organic matrix and diffusivity.

Next, to minimize the scatter penalties per bond converted, it can be advantageous to introduce a polymerization retarder to shift the development time to be longer than the exposure time. This is because the dominant physical mechanism for recording-induced scatter in organic media is the formation of so-called parasitic or noise gratings.[31] These noise gratings are initially weakly seeded by point scattering sites in the media, and are then self-amplified by the index response that occurs during the recording exposure. With the introduction of a polymerization retarder, however, most of the polymerization occurs in the dark post-exposure, so that this feedback loop is suppressed.[74] Taking this approach to its extreme, fully latent recording schemes have been proposed, in which exposure and development are completely time-separated.[75]

Finally, the shrinkage penalty per bond converted can be minimized by utilizing cationic ring-opening writing chemistries, in which this shrinkage is partially compensated by a volume increase due to ring-opening.[36] The use of a cationic rather than a radical polymerization also means that recording is not inhibited by oxygen, and that it continues to exhibit a linear response even at high exposure intensities. This enables architectures in which a moving media layer is addressed by a pulsed laser or a laser with nanosecond-scale external modulation, as is required for high-throughput micro-holographic recording. Commercial media Aprilis[76] achieved $\Delta n \sim 0.1$ with negligibly small shrinkage, ~0.04%, although the cationic writing chemistry makes it difficult to suppress unwanted dark polymerization.

Free radical ring-opening polymerization[77] has the potential to achieve the best of both worlds: compensation of volume shrinkage to within a remarkable 0.02%, and also suppression of dark polymerization. However, limited explorations of this writing chemistry to date have yielded only $\Delta n \sim 1 \times 10^{-3}$ with sensitivity of 1.1×10^{-3} cm^2/J.

RECORDING KINETICS

Unique Metrology Challenges

The design choices discussed so far determine the Δn that would be achievable in the case of perfect recording fidelity. But the actual fidelity and spatial resolution are limited (often severely, as we will see below) due to the reaction/diffusion kinetics of recording. These limits must be taken into account by any program for rational design of media.

However, quantitative characterization of the kinetics is challenging, since the processes of interest are not only highly coupled, but also typically occur at submicron spatial scale and submillimolar concentration. Conventional metrology techniques, such as FT-IR spectroscopy and differential scanning calorimetry, are of limited utility here, and so a new suite of specialized characterization techniques has been developed. In this section, we first review the basic reaction/diffusion mechanisms for recording, and then briefly survey the historical development of these specialized metrology techniques. Finally we offer a more quantitative account of how these kinetics limit the recording fidelity and spatial resolution.

Establishing a Diffusional Mechanism for Index Modulation

Historically, the first step in understanding reaction/diffusion kinetics was simply identifying a diffusion-driven mechanism for index response. Photopolymer holographic media were first realized in a liquid resin system with high-index metal acrylates and an acrylamide binder.[78] A diffusional mechanism was later proposed, and grating growth times were found to be consistent with independently measured diffusivities.[79] Other early photopolymer media were not liquid resins, but instead formed a glassy host matrix, either polyester[80] or PMMA.[81,82] Index modulation was due not to photo-crosslinking as initially speculated, but rather diffusion

of residual free monomer,[83] and thus long development times (up to 200 h in the latter case) could be attributed to the low diffusivity of the PMMA matrix.

A final important class of early diffusion-driven media, including early Lucent media, are initially liquid but begin to crosslink upon photoexposure.[84,85] The same photochemistry initiates polymerization of both crosslinkers and high-index monomers. But the crosslinkers are more highly reactive, so that a uniform precure will preferentially form a crosslinked matrix, while leaving the high-index monomer mostly unreacted until a later patterned exposure. A disadvantage of this approach is that the two processes are not perfectly orthogonal: inevitably some high-index monomer is uniformly polymerized during the precure, thereby reducing the available index modulation. Another disadvantage is that diffusivity typically decreases by orders of magnitude as conversion runs from 0 to 100%, so that small variations in the initial matrix-forming step can lead to undesirable large variations in recording kinetics.

In all of these single-chemistry systems, in-diffusion of writing monomer toward the exposed regions leads to volume displacement of the inert binder or matrix toward the unexposed regions. This counter-diffusion of index-contrasting components has been shown to be the dominant source of index modulation, as opposed to densification of writing polymer, which makes at most a negligible contribution to index modulation.[84,86,87]

Based on this insight, the Lucent group presents a quantitative model of index modulation which assumes ideal volume displacement.[88] This article notes that, on this assumption, the observed Δn should be proportional to the index difference of the components, $(n_{\text{writing polymer}} - n_{\text{binder}})$. Later, this same proportionality is conclusively demonstrated for Lucent two-chemistry media,[72] although the connection to matrix displacement is not drawn explicitly. Finally, a direct quantitative observation of matrix displacement is realized by Kagan et al. using confocal Raman microspectroscopy.[89]

Metrology Strategies

Having identified the basic reaction/diffusion processes of interest in these photopolymer media, we now consider specialized techniques to characterize them. The most fundamental such technique is to monitor the diffraction efficiency of a developing holographic grating, using a Bragg-matched readout beam. The diffraction efficiency can readily be converted to an index modulation via Kogelnik's coupled-wave theory,[90] and indirectly yields information about reaction and diffusion timescales.[91]

The crucial advantage of this coherent measurement is that it yields a high SNR, real-time, *in situ* measurement of gratings with as low as sub-micron spatial scales and sub-millimolar concentrations. In contrast, conventional techniques for characterizing reaction/diffusion kinetics, such as FT-IR spectroscopy or differential scanning calorimetry, face signal-to-noise challenges when attempting to characterize two-chemistry media, since the writing chemistry of interest comprises such a small fraction of the material.

It must be remembered, however, that this Bragg measurement only gives information about a single spatial frequency of the index modulation (typically the fundamental), and cannot detect a spatially uniform component of the index change. Lastly, the Kogelnik relationship between diffraction efficiency and index modulation assumes a low-scatter grating with uniform phase, amplitude, and spatial frequency throughout its depth. Thus it can only be applied quantitatively to media that already have relatively high performance, and is of limited utility in optimizing media with, for example, high volume shrinkage.

An elaboration of this technique for quantifying reaction/diffusion kinetics is put forward in the Nonlinear Polymerization-Driven Diffusion (NPDD) model, developed for acrylamide media in an influential series of papers by Sheridan et al (summarized in Ref. 92). In this media, as in many others, reaction and diffusion take place on overlapping timescales, and so independent measurement of their rate coefficients is difficult. Instead, the NPDD strategy extracts many of these rate coefficients as simultaneous free fit parameters from Bragg-monitored grating growth curves. A tractably simple set of equations for fitting is obtained by expanding the coupled reaction/diffusion equations as a spatial harmonic series and retaining only the first few terms. This corresponds neatly to the successive spatial harmonics probed by measurements of successive Bragg orders. Thus, this technique leverages the high signal-to-noise ratio of Bragg measurements into precise values for fit parameters.

At the heart of the model is a proposed set of reaction/diffusion physics. Most notably, the model proposes that growing acrylamide chains are promptly immobilized due to entanglement, but that the radical tips of these still-growing chains then undergo reaction-diffusion over relatively large distances, characterized by a "nonlocal parameter" $\sigma^{1/2} \sim$ 60 nm. This mechanism generates diffusional blurring and gives rise to the spatial resolution limit of the media.[93] This set of reaction paths is extended in later work, to capture additional physics including: bimolecular termination[94] and primary termination; inhibiting species such as oxygen;[95] depletion of initiator during long exposures;[96] chain transfer;[97] and postexposure dark polymerization. Recent versions of the model also incorporate local slowing of diffusion with increasing degree of conversion.[98]

The same approach is extended to DuPont media by Wu and Glytsis.[99] Here, the harmonic expansion is replaced by full FDTD modeling, and the Kogelnik equation for diffraction efficiency is replaced by rigorous coupled-wave analysis (RCWA), but the results are qualitatively similar.

One fundamental challenge of this approach is that even a good fit to experimental data cannot in general be taken as validation of the underlying physical assumptions and set of reaction paths. For example, Martin et al.[100,101] propose a

somewhat different underlying physical process for diffusional blurring of small-pitch gratings. The Toal model attributes blurring to diffusion of short mobile chains, whereas the Sheridan model attributes blurring to reaction-diffusion of immobilized chains. Both models yield acceptably good fits to Bragg data; in other words, the fitting procedure does not decisively resolve the question of what is the fundamental physical mechanism behind the media resolution limit.

This general concern has been addressed, in more recent work in the NPDD framework, by turning toward independent measurements of some parameter values. For example, Gallego et al.[102] note the difficulty of disentangling reaction and diffusion effects with overlapping timescales, and instead separate these timescales by increasing the grating pitch to 80 μm, so that diffusion across a fringe becomes much slower than reaction. Sheridan et al have also demonstrated diffusivity measurements using this same approach,[103] or using entirely non-holographic techniques such as gravimetry.[104] Similarly, photoinitiator quantum efficiency has also been studied via independent non-holographic measurements.[105]

This turn toward independent measurements has culminated in the extension of the NPDD framework to other classes of media where a large body of characterization work is already available—first to the original Trentler media,[106] and more recently to Bayer two-chemistry media.[107] In the latter case, many initial parameter values for the iterative fit procedure are drawn from the results of independent experiments. These include not only the component refractive indices, but also the polymerization rate coefficient k_p (from pulsed-laser polymerization in combination with size-exclusion chromatography[108]) and the conversion-induced slowing coefficient α (from shear modulus measurements). Finally, the set of parameters obtained from an iterative fit is further validated against experimental results at different grating pitches.

Reaction/Diffusion Kinetics Lead to Imperfect Recording Fidelity

Ultimately, the details of the recording kinetics are of practical importance insofar as they produce deviations from linear (i.e. perfect fidelity) index response. Several different general mechanisms cause these deviations, depending on the recording spatial frequency.

First, recording at low spatial frequencies can be hindered as timescales of reaction and in-diffusion become coupled. The effect of this coupling, as observed in Ref. 109 and rigorously formalized in the foundational Zhao and Mouroulis article,[110] is as follows. If individual exposures are sufficiently strong to locally deplete writing monomer in the bright regions, then subsequent polymerization will preferentially happen at the edges of bright regions, fueled by monomer in-diffusing from the dark regions. This generates characteristic "rabbit ears" features comprising higher harmonics rather than the intended fundamental spatial frequencies.

Even worse, this nonlinear regime often cannot be avoided in practical applications. Local depletion of monomer is unavoidable for applications requiring strong individual features, such as waveguides and display holograms. The overlapping timescales for reaction and diffusion are sometimes unavoidable as well, since both of these timescales must be short in order to ensure good sensitivity and development speed respectively.

Later extensions of the Zhao and Mouroulis model incorporate additional physics such as continued dark polymerization.[111] Its design implications are explored in more depth by Schilling et al.[85] concluding that "The optimal material would strike a fine balance between the opposing material requirements of dimensional rigidity and fast diffusion time scales." High crosslink densities yield appealing bulk mechanical properties, but an undesirably low diffusivity that prevents complete polymerization of writing monomer.

Low spatial frequency recording can also be hindered by a second mechanism, in which polymerization-induced slowing interrupts monomer diffusion across large features. The Zhao and Mouroulis analysis can be extended to account for such conversion-dependent diffusivity.[112] Free volume theory provides simple expressions for the dependence of both reaction and diffusion rates on local degree of conversion; these have been incorporated into fully quantitative kinetic models to achieve remarkably good agreement with experiment.[88]

Next, recording at high spatial frequencies can also be suppressed, through the general mechanism of diffusional blurring. Here some photogenerated species undergoes significant diffusion from bright regions into dark regions before becoming immobilized. The amount of blurring is expected to scale as $1/\Lambda^2$, where Λ is the spatial period, since this is the scaling for the time to diffuse across a fringe.[113]

This scaling enables the prediction of media resolution limits from experimentally accessible measurements at lower spatial frequencies. Furthermore, this scaling is independent of the particular physical mechanism for diffusional blurring. Figure 2 shows experimental confirmation of this scaling in various media formulations. It should be emphasized that this scaling obtains regardless of the underlying physical mechanism for diffusional blurring. For example, in Ref. 114 blurring is attributed to diffusion of short mobile chains, but in Ref. 97 it is attributed to reaction-diffusion of the radical tips of fixed chains. We also note that the impact of grating spatial period on obtained refractive index contrast is only rarely reported in the materials literature and that this is a potentially uncontrolled variable in the materials comparisons that follow.

The above mechanisms, taken together, give each material a characteristic transfer function in the spatial frequency domain. This can lead to undesirable effects, including strongly reduced diffraction efficiency of high-spatial-

frequency reflection holograms (as in e.g. display or spectral filter applications). But if the transfer function is well matched to the desired recording spatial frequencies, it can afford suppression of scatter noise (at higher spatial frequencies) and recording beam aberrations (at lower spatial frequencies). These effects will be neglected in the survey of materials below; instead we consider the usable Δn only at the spatial frequency of the reported experiments.

Finally, even after the above mechanisms have all been accounted for, some additional waste mechanisms are present regardless of spatial frequency. For instance, we have previously argued that, in some two-chemistry media, chain transfer effects give rise to short unattached chains of writing polymer, which then diffuse away to produce an unwanted uniform background index change.[114]

FORMULA LIMIT CONCEPT

A full understanding of the recording kinetics of a candidate media formulation, then, typically requires a sustained investigation, drawing on multiple experimental techniques. However, the goal of those recording kinetics is primarily to cause segregation of species whose refractive index contrast gives rise to the desired material index modulation. Thus, even in the absence of comprehensive kinetic model, it is possible to obtain salient insights into the recording fidelity simply by comparing the Δn observed to that calculated from the Lorentz-Lorenz equation assuming 100% segregation of the formulated components. We refer to this upper bound on index contrast as the "formula limit." The ease of this calculation renders it suitable for rapid surveys of multiple candidate formulations.

We define the "formula limit" as the theoretically achievable index modulation, in the limit of ideal spatial patterning of all components. "Ideal" index patterning is taken to mean linearly proportional to the incident intensity pattern. Since sinusoidal intensity patterns are naturally generated by interference and Bragg selectivity in these thick holograms restricts diffraction to a single sinusoidal spatial frequency of the index, the natural profile for analysis is a sinusoid. This motivates the traditional harmonic analysis approach[92] in which non-fundamental harmonics of the intensity are recorded due to nonlinear kinetics. These harmonics do not Bragg match, do not contribute to diffraction and thus are not usable, as defined here. We note that this harmonic analysis can be applied to non-sinusoidal intensity patterns via Fourier decomposition of the intensity.

This limit on maximum possible index contrast can be straightforwardly derived using the Lorentz-Lorenz relation for the refractive index of a mixture, n, consisting of two species specified by their volume fraction φ_i and refractive index n_i[116] as

$$\frac{n^2-1}{n^2+2}=\varphi_1\frac{n_1^2-1}{n_1^2+2}+\varphi_2\frac{n_2^2-1}{n_2^2+2}\,.$$

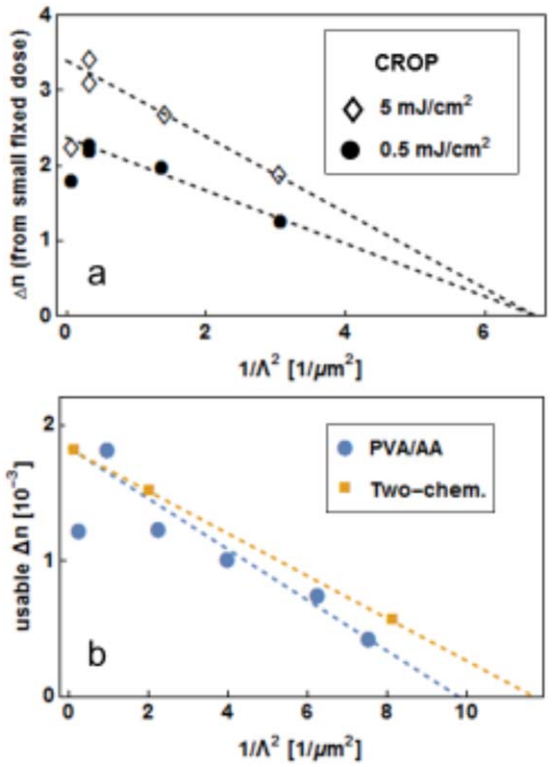

FIGURE 2 Spatial frequency variation of index response Δn, showing that different classes of media all exhibit the same $1/\Lambda^2$ scaling that is characteristic of diffusional blurring mechanisms. To make this scaling visually apparent, we take data points from the referenced works and plot them against $1/\Lambda^2$ where Λ is grating pitch. Dashed lines are fits to these data points; their x-intercepts indicate the media spatial resolution limit. (a) CROP media;[115] it can now readily be seen that two different exposure intensities yield the same resolution limit, even though it falls outside the range of experimentally accessible spatial frequencies. (b) Acrylamide media[97] and two-chemistry media.[114]

Assuming ideal mixing of incompressible species, $\varphi_1+\varphi_2=1$ and weak index contrast $|n_2-n_1| \ll n_{1,2}$, this is well approximated as:[97]

$$\begin{aligned} n&=n_1\varphi_1+n_2\varphi_2\\ &=n_1\varphi_1+n_2(1-\varphi_1)\\ &=n_2+(n_1-n_2)\varphi_1\,. \end{aligned}$$

This formula readily generalizes to multiple mobile species such as a reactive monomer and an inert binder. In the common case of a single mobile species such as a mobile photopolymerizable monomer in a crosslinked polymerized matrix, we may identify $n_{1,2}$ as the refractive index of the writing polymer and matrix, respectively and φ_1 as the formulated volume fraction of the writing monomer after polymerization. Then, $\Delta n \equiv n-n_2$ is the largest possible peak to mean index contrast possible when a sinusoidal intensity pattern causes 100% segregation of the writing polymer such that zero remains at the center of the dark fringe and the volume fraction at the peak of the bright fringe is doubled. We thus define

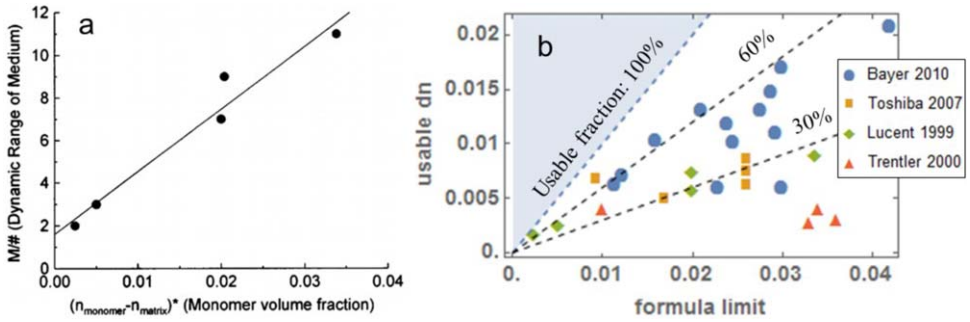

FIGURE 3 (a) Usable Δn of various formulations (expressed as *M*/#), plotted against a quantity that is equal to the "formula limit" as defined here. Reproduced from Ref. 72 with permission from OSA. (b) The data points from (a), along with data from other similar two-chemistry formulations, from the early Trentler et al. article[117] to the more recent Toshiba[118] and Bayer[119] patents. The improvements in usable Δn within the last decade are evidently due to increases in usable fraction, rather than formula limit.

$$\Delta n_{\text{formula}} = \left(n_{\text{writing polymer}} - n_{\text{matrix}}\right)\varphi_{\text{writing polymer}}.$$

This approximate linear formula is accurate to better than 4% when the volume fraction of writing polymer is low (<10 vol %) and the species index contrast is weak (<0.1), as is the case for typical two-chemistry media. However, in the following sections we will instead calculate the formula limit using the full Lorentz-Lorenz relation,[116] rather than this linear approximation, to ensure that our analysis is valid even for single-chemistry media with volume fraction ratios near 50/50.

In practice, the index modulation Δn obtained by most reported materials is only some fraction of this limit; we call this the "usable fraction." The remaining fraction must correspond to writing polymer that is not distributed with the desired spatial patterning, due to the recording nonlinearities discussed above and any non-ideal recording conditions such as vibration, imperfect beam ratio, insufficient development time etc. However, since the maximum possible refractive index contrast can be simply calculated as explained above, the fraction that is not ideally patterned reveals the relative magnitude of these deleterious effects. This wasted fraction is important from a materials design perspective, not only because it fails to contribute to usable Δn, but also because it does still actively contribute to unwanted volume shrinkage and scatter.

To illustrate the ease and utility of this calculation, we will perform it for a representative set of formulations of academic and commercial interest, whose component indices and volume fractions are already reported. This quantitative review cannot, of course, capture the many intricate experimental details of each reported result that may have contributed to the achieved index contrast; we simply summarize here what was reported and note salient trends. As a starting point for visualizing these results, we consider a plot from Ref. 72 [Fig. 3(a)], where usable Δn is plotted against the quantity identified here as the formula limit. Each data point on this plot represents a media formulation with slightly different components, but the same underlying chemistry. The fact that the points fall roughly on a straight line means that the usable fraction is roughly equal in all of these formulations. This roughly linear behavior, which will be exhibited again below, indicates that the recording kinetics are not strongly affected by the substitution of new components with different index but the same reactive groups. This supports the concept of the usable fraction of the formula limit as a design metric that is primarily dependent on chemical composition but largely independent of specific concentrations.

Next, Figure 3(b) compares this result to later generations of two-chemistry media, revealing that their enhanced Δn is primarily due to improvements in the usable fraction, rather than the formula limit. These improvements have been qualitatively explained in terms of changes in the recording kinetics. For example, the matrix crosslink density can be tuned to optimize the relative rates of reaction and diffusion.[119] Alternatively, the rate of immobilization of growing polymer chains can be improved by incorporating additional reactive sites into to the matrix.[114] Even greater control of immobilization can in principle be achieved using, for example, thiol-click writing chemistry; an early proof of concept[120] is included in Figure 4 below. The formula limit analysis presented here enables a meaningful comparison of these various modifications, even in the absence of comprehensive kinetic models.

This formula limit analysis can also be fruitfully applied to single-chemistry media. For example, Ref. 86 explores the same chemistry later used in DuPont commercial media. Various pairings of candidate writing monomers and binders are evaluated [Fig. 4(a)], concluding that high-index binders should be paired with low-index monomers, and vice versa. However, an additional trend becomes apparent when the results are plotted in terms of usable fraction [Fig. 4(b)]: all formulations incorporating a given binder tend to have roughly the same usable fraction, even as their absolute Δn varies widely. Furthermore, the binders with the highest usable fractions are those with the lowest reported small-molecule diffusivities [Fig. 4(b) inset], whereas high

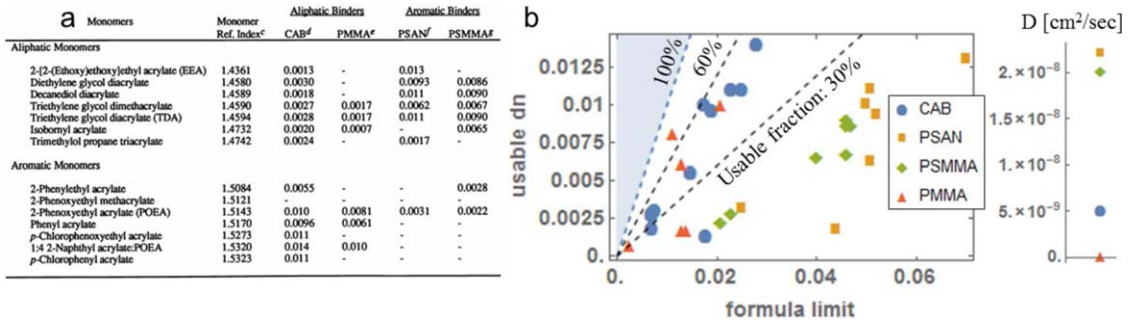

a Monomers	Monomer Ref. Index[c]	Aliphatic Binders CAB[d]	PMMA[e]	Aromatic Binders PSAN[f]	PSMMA[g]
Aliphatic Monomers					
2-[2-(Ethoxy)ethoxy]ethyl acrylate (EEA)	1.4361	0.0013	-	0.013	-
Diethylene glycol diacrylate	1.4580	0.0030	-	0.0093	0.0086
Decanediol diacrylate	1.4589	0.0018	-	0.011	0.0090
Triethylene glycol dimethacrylate	1.4590	0.0027	0.0017	0.0062	0.0067
Triethylene glycol diacrylate (TDA)	1.4594	0.0028	0.0017	0.011	0.0090
Isobornyl acrylate	1.4732	0.0020	0.0007	-	0.0065
Trimethylol propane triacrylate	1.4742	0.0024	-	0.0017	-
Aromatic Monomers					
2-Phenylethyl acrylate	1.5084	0.0055	-	-	0.0028
2-Phenoxyethyl methacrylate	1.5121	-	-	-	-
2-Phenoxyethyl acrylate (POEA)	1.5143	0.010	0.0081	0.0031	0.0022
Phenyl acrylate	1.5170	0.0096	0.0061	-	-
p-Chlorophenoxyethyl acrylate	1.5273	0.011	-	-	-
1:4 2-Naphthyl acrylate:POEA	1.5320	0.014	0.010	-	-
p-Chlorophenyl acrylate	1.5323	0.011	-	-	-

FIGURE 4 (a) Performance of various candidate formulations, using the same basic chemistry as later DuPont commercial media. Reproduced from Ref. 86 with permission from SPIE. (b) The same data, plotted against formula limit, showing that all formulations with a given binder tend to have a similar usable fraction despite their widely differing absolute Δn. Inset: reported diffusivities D for each binder. Good usable fraction is associated with low D, in contrast to some other systems.

diffusivities are believed to be essential in many other photopolymer systems.

Next, a similar analysis can be performed for many of the other material design strategies described above, including ring-opening writing chemistries; these results are summarized in Figure 5. In particular, it is apparent that the ring-opening formulations reported in the literature, either cationic or radical, have relatively low usable fractions. (Evidence that diffusional blurring is a significant source of waste is reported elsewhere.[115]). Thus, if these fractions can be improved (as was achieved for conventional radical writing chemistries via engineering new immobilization pathways, above), a dramatic enhancement of Δn will be possible without any sacrifice of shrinkage performance.

Another general strategy for enhancing dynamic range is to dope the media with some freely diffusing but chemically inert species that will be displaced into the unexposed regions as writing polymer accumulates in the exposed regions. The counter-diffusant can be either low-index[122] or high-index,[123,124] as long as it is strongly index-contrasting with the writing polymer.

Inorganic nanoparticles (NPs) are appealing candidates to achieve this high index contrast.[125] Furthermore, a high volume fraction of NPs also affords other advantages, including improved thermal stability and reduced polymerization-induced shrinkage.[126] A significant challenge in NP-doped media is controlling the optical turbidity due to Rayleigh scattering from the highly index-contrasting NPs or NP aggregates. This scattering is minimized by using small (i.e. hydrodynamic diameter <10 nm) nanoparticles, with organic coatings to reduce aggregation. The size of the organic coating is subject to a design tradeoff: a high volume fraction of organics "...increases the compatibility of the NP with organic media, but decreases strongly the average refractive index of the NP and, consequently, the refractive index modulation...."[127] By appropriately managing this tradeoff, NP-doped media have simultaneously achieved very low optical scatter and good index modulation of 5.3×10^{-3}.[126]

This result and others are summarized in Figure 6. Just as in the case of the two-chemistry media discussed above, the last decade has seen dramatic improvements in Δn, primarily due to increases in usable fraction, rather than increases in formula limit. For example, it has recently been shown[132]

a

Monomer Functionality[a]	Binder[b]	PAG[c]	Threshold[d] (mJ / cm²)	Sensitivity (cm² / mJ)[e]	n_1[f]
2	710	OCTO	26	0.019	0.002
2	705	OCTO	22	0.027[g]	0.0036
2	ps22107	OCTO	8.5	0.027	
2	ps20019	OCTO	2.5	0.051	
2	Con	OCTO	4.5	0.065	
[illegible]	[illegible]	[illegible]	[illegible]	[illegible]	[illegible]
2	710	MPIB	7.5	0.073	0.004
2	705	MPIB	6	0.104	0.0064
2,4	710	OCTO	19	0.019	0.0024
2,4	710	OCTO	5.5[h]	0.032[h]	0.0026
2,4	705	MPIB	1.5	0.067	> 0.0026
2	PMNS	OCTO	30	0.05	0.003
2	PMNS	MPIB	2	0.06	0.003

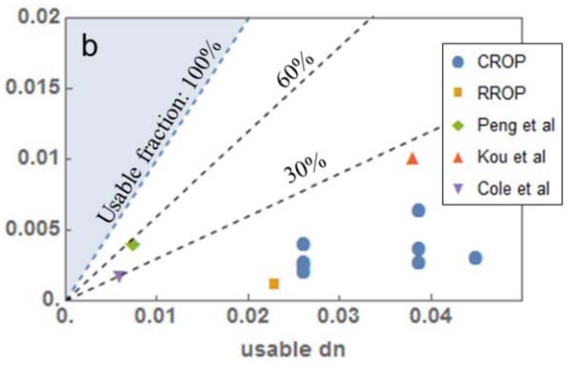

FIGURE 5 (a) Measured performance of various early CROP formulations. Reproduced from Ref. 36 with permission from SPIE. (b) The same data as (a), plotted in terms of usable Δn versus estimated formula limit, along with reported data for a variety of other design strategies: Choi et al. (RROP),[77] Peng et al. (thiol-click),[120] Cole and Trentler (thermoplastic matrix),[38] Kou et al. (dendritic binder).[121] See Supporting information for details.

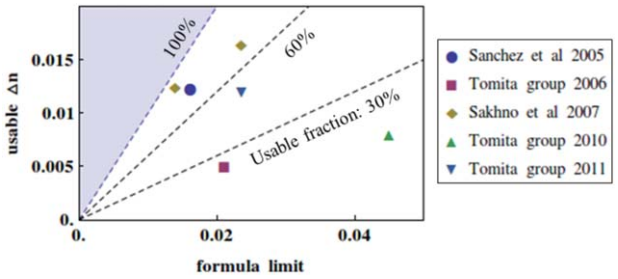

FIGURE 6 Usable Δn of nanoparticle-doped media, plotted against formula limit to show that high usable fractions are achievable. Respective sources, including both organic and inorganic nanoparticles.[127-131]

that the addition of a chain transfer agent to a NP-doped formulation results in a remarkable twofold improvement in usable Δn, to as high as 0.016, without any increase in the nanoparticle loading (or, therefore, any increase in the formula limit). Instead, this improvement is attributed to more favorable reaction/diffusion kinetics, which also result in improved index response at high spatial frequencies.[133]

Other candidates for highly index-contrasting counter-diffusants are organic, including hyperbranched-polymer nanoparticles,[128] with reported index as high as 1.72[134] and fluorinated urethane oligomers with index as low as ~1.4.[135]

A similar counter-diffusion mechanism enables photopatterning in polymer-dispersed liquid crystals, whereby the liquid crystals are displaced into unexposed regions and form microdomains.[136] These are an important class of materials due to their capacity for dynamic electrically switchable diffractive elements.[137] However, optical scatter from the liquid crystal microdomains remains a fundamental problem, especially since modifications to reduce the microdomain size (e.g. via higher crosslink densities) also tend to increase the required switching voltage. A more detailed treatment of nanoparticle and liquid crystal counter-diffusants is outside the scope of this review, but since their distribution is governed by the distribution of writing polymer, the design strategies put forward here will be directly applicable to these cases as well.

CONCLUSION

We have shown that the formula limit and usable fraction can be readily estimated for a broad range of media in the existing literature, without requiring a comprehensive investigation into their recording kinetics. There are, of course, limits to the applicability of this analysis. First, it requires knowledge of the mixing rule. Here we have assumed nearly perfect 1:1 volume mixing, consistent with all of the relatively few mixing studies in two-chemistry media. If, however, a significant density modulation occurs, the calculated usable fraction will be in error. In the usual case of high-index writing monomer, this density modulation will add up in phase with the expected compositional modulation, and so the analysis presented here will overestimate the usable fraction.

Second, this analysis requires precise knowledge of the media composition. This condition may not be met in, for instance, the acrylamide media discussed above, which retain anywhere from order 1% to order 10% water at the time of recording, strongly depending on film thickness and the exact details of the drying procedure[138]. A further complication is that acrylamide becomes more hydrophilic upon polymerization, so that in some cases the media layer postrecording absorbs significant additional moisture from the air.[139] Worse, since water is highly index-contrasting, even modulations of the water concentration as slight as 1% (with respect to overall volume) would be sufficient to produce index modulations of the same order (10^{-3}) as the total observed index modulation. This suggests that a detailed treatment of water concentration modulations could be a fruitful addition to the extensive work in quantitative modeling of acrylamide media.

Despite these limitations, formula limit analysis affords useful information about recording fidelity in a broad range of significant media formulations. In particular, it shows that many media formulations still have significant room for optimization of usable fraction. Some optimization strategies have already been demonstrated (e.g. matrix-attached protected radical groups), and other strategies for matrix-attached functional groups also appear promising (e.g. acrylate writing chemistry, with additional acrylate groups tethered to the matrix).

However, this formula limit analysis also provides an estimated upper bound on future performance improvements in holographic media. Considering each successive term in the formula limit expression, we first note that the upper bound on the volume fraction of index-contrasting component is 0.5. Next we consider the achievable index contrast between components, constrained in general by the requirement of good solubility in the organic polymer matrix. Index as high as ~1.7 has been demonstrated in organic writing monomers, and a similarly high index has been demonstrated in surface-modified inorganic nanoparticles (e.g. 1.72 in Ref. 140) Conversely, index as low as ~1.4 has been demonstrated in fluorinated counter-diffusants. Finally, the usable fraction can by definition be at most 100%.

Thus, an upper bound on plausibly achievable Δn is given by a hypothetical optimized material with equal volume fractions of two perfectly counter-diffusing components with $n = 1.4$ and 1.7, yielding a usable Δn of ~0.15. Existing media, with reported Δn in excess of 0.04,[141] already achieve a significant fraction of this theoretical upper bound. This analysis affords a better understanding of constraints on the application space for diffusion-driven photopolymers, and highlights the growing importance of design strategies which address other aspects of performance besides Δn, such as matrix-tethered functional groups for increased spatial and temporal control of photopolymerizations.

ACKNOWLEDGMENTS

This material is based upon work supported by the National Science Foundation under grant numbers 1307918 and 1240374. B. Kowalski is a postdoctoral researcher at the Air Force Research Lab at Wright-Patterson AFB. His research interests include diffractive optical elements as realized in either liquid crystal elastomers or conventional holographic photopolymers. He holds degrees from the University of Colorado and Kenyon College. R. McLeod is Department Chair and the Richard and Joy Dorf Endowed Professor of Electrical, Computer and Energy Engineering at the University of Colorado Boulder and a topical editor for Optics Letters. His research group specializes in the interaction of light and organic materials with applications to lithography, integrated optics, computational imaging and cellular biology. He holds graduate degrees from Montana State University, University of California, and the University of Colorado.

REFERENCES AND NOTES

1 H. J. Coufal, G. T. Sincerbox, D. Psaltis, Holographic Data Storage; Springer-Verlag: New York, **2000**.

2 A. Hoskins, B. Ihas, K. Anderson, K. Curtis, *Jpn. J. Appl. Phys.* **2008**, *47*, 5912–5914

3 R. R. McLeod, A. J. Daiber, M. E. McDonald, T. L. Robertson, T. Slagle, S. L. Sochave, L. Hesselink, *Appl. Opt.* **2005**, *44*, 3197–3207.

4 M. R. Ayres, R. R. McLeod, *Appl. Opt.* **2009**, *48*, 3626–3637.

5 R. R. McLeod, *JOSA B.* **2009**, *26*, 308–317.

6 E. Mihaylova, I. Naydenova, S. Martin, V. Toal, *Appl. Opt.* **2004**, *43*, 2439–2442.

7 D. Lanteigne, T. Hudson, D. Gregory, *Appl. Opt.* **1987**, *26*, 184–185.

8 S. Yiou, F. Balembois, P. Georges, J. Huignard, *Opt. Lett.* **2003**, *28*, 242–244.

9 A. Heifetz, J. T. Shen, J. K. Lee, R. Tripathi, M. S. Shahriar, *Opt. Eng.* **2006**, *45*, 025201–025201.

10 A. C. Urness, E. D. Moore, K. Kamysiak, M. Cole, R. R. McLeod, *Light Sci. Appl.* **2013**, *2*, e56.

11 R. Olson, N. Mamalis, B. Haugen, *Curr. Opin. Ophthalmol.* **2006**, *17*, 72–79.

12 A. C. Sullivan, M. W. Grabowski, R. R. McLeod, *Appl. Opt.* **2007**, *46*, 295–301.

13 B. L. Booth, J. E. Marchegiano, C. T. Chang, R. J. Furmanak, D. M. Graham, R. G. Wagner, *Photonics West*. Proc. SPIE 3005, Optoelectronic Interconnects and Packaging IV, pp. 238–251 (April 4, 1997, San Jose, CA) **1997**.

14 A. S. Kewitsch, A. Yariv, *Opt. Lett.* **1996**, *21*, 24–26.

15 B. L. Booth, J. E. Marchegiano, In Optical Communication, 1988 (ECOC 88), Fourteenth European Conference; 1988; pp 589–590, Conference Publication no. IET (September 11, 1988, Brighton) 292.

16 Q. Huang, P. Ashley, *Appl. Opt.* **1997**, *36*, 1198–1203.

17 J. M. Wang, L. Cheng, A. A. Sawchuk, *Appl. Opt.* **1993**, *32*, 7148–7154.

18 E. D. Moore, A. C. Sullivan and R. R. McLeod, In Photonic Devices+ Applications; International Society for Optics and Photonics; Proc. SPIE 7053, Organic 3D Photonics Materials and Devices II, p. 705309 (August 28, 2008, San Diego, CA) **2008**; pp 705309–705309.

19 D. D. Do, N. Kim, J. W. An, K. Y. Lee, *Appl. Opt.* **2004**, *43*, 4520–4526.

20 I. P. Kaminow, H. P. Weber, E. A. Chandross, *Appl. Phys. Lett.* **2003**, *18*, 497–499.

21 V. K. S. Hsiao, W. D. Kirkey, F. Chen, A. N. Cartwright, P. N. Prasad, T. J. Bunning, *Adv. Mater.* **2005**, *17*, 2211–2214.

22 X. Yang, X. Pan, J. Blyth, C. R. Lowe, *Biosens. Bioelectron.* **2008**, *23*, 899–905.

23 M. E. Baylor, B. W. Cerjan, C. R. Pfiefer, R. W. Boyne, C. L. Couch, N. B. Cramer, C. N. Bowman, R. R. McLeod, *Opt. Mater. Express* **2012**, *2*, 1548–1555.

24 J. M. Tedesco, L. A. Brady, W. S. Colburn, *SID Int. Symp. Dig. Tech. Pap.* **1993**, *24*, 29–29.

25 W. Chao, S. Chi, *J. Opt.* **1998**, *29*, 95–103.

26 J. M. Castro, D. Zhang, B. Myer, R. K. Kostuk, *Appl. Opt.* **2010**, *49*, 858–870.

27 M. A. Klug, C. Newswanger, Q. Huang, M. E. Holzbach, U.S. Patent 7,227,674, June 5, Zebra Imaging, Inc **2007**.

28 D. Jurbergs, F. K. Bruder, F. Deuber, T. Fäcke, R. Hagen, T. Hönel, T. Rölle, M. S. Weiser, A. Volkov, *Proc. SPIE* **2009**, *7233*, 72330K–723K10.

29 F. H. Mok, G. W. Burr, D. Psaltis, *Opt. Lett.* **1996**, *21*, 896–898.

30 P. Munk, T. Aminabhavi, Introduction to Macromolecular Science, 2nd ed.; Wiley-Interscience, **2002**; New York: Wiley, pp 152.

31 A. Beléndez, A. Fimia, L. Carretero, F. Mateo, *Appl. Phys. Lett.* **1995**, *67*, 3856–3858.

32 Y. Takashima, L. Hesselink, *Jpn. J. Appl. Phys.* **2009**, *48*, 03A004.

33 A. Fimia, N. Lopez, F. Mateos, R. Sastre, J. Pineda, F. Amat-Guerri, *J. Mod. Opt.* **1993**, *40*, 699–706.

34 K. Curtis, L. Dhar, A. Hill, W. L. Wilson, M. Ayres, Holographic Data Storage: From Theory to Practical Systems; New York: Wiley, **2011**.

35 C. Ye, K. T. Kamysiak, A. C. Sullivan, R. R. McLeod, *Opt. Express* **2012**, *20*, 6575–6583.

36 D. A. Waldman, R. T. Ingwall, P. K. Dhal, M. G. Horner, E. S. Kolb, H. Y. S. Li, R. A. Minns, H. G. Schild, *Proc. SPIE.* **1996**, *2689*.

37 R. K. Kostuk, *Appl. Opt.* **1999**, *38*, 1357–1363.

38 M. C. Cole, T. J. Trentler, U. S. Patent 8,071,260, December 6, **2011**, InPhase Technologies, Inc.

39 P. Wang, B. Ihas, M. Schnoes, S. Quirin, D. Beal, S. Setthachayanon, Proc. SPIE 5380, Optical Data Storage 2004, pp. 283–288 (September 9, 2004, Monterey, CA) **2004**.

40 L. Dhar, M. G. Schnoes, T. G. Wysocki, H. Bair, M. Schilling, C. Boyd, *Appl. Phys. Lett.* **1998**, *73*, 1337–1339.

41 D. P. Nair, N. B. Cramer, J. C. Gaipa, M. K. McBride, E. M. Matherly, R. R. McLeod, R. Shandas, C. N. Bowman, *Adv. Func. Mat.* **2012**, *22*, 1502–1510.

42 R. R. Gattass, E. Mazur, *Nat. Photonics.* **2008**, *2*, 219–225.

43 A. Zoubir, C. Lopez, M. Richardson, K. Richardson, *Opt. Lett.* **2004**, *29*, 1840–1842.

44 A. M. Kowalevicz, V. Sharma, E. P. Ippen, J. G. Fujimoto, K. Minoshima, *Opt. Lett.* **2005**, *30*, 1060–1062.

45 T. Gerke, R. Piestun, *Nat. Photonics* **2010**, *4*, 188–193.

46 M. P. Bernal, P. M. Lundquist, C. Poga, H. Coufal, R. K. Grygier, R. G. DeVoe, Y. Jia, *Opt. Lett.* **1996**, *21*, 890–892.

47 Photorefractive Materials and Their Applications; P. Günter, J.-P. Huignard, Eds.; Springer-Verlag: Berlin, **1989**.

48 W. E. Moerner, S. M. Silence, F. Hache, G. C. Bjorklund, *Josa B.* **1994**, *11*, 320–330.

49 S. Kawata, Y. Kawata, *Chem. Rev.* **2000**, *100*, 1777–1788.

50 C. Erben, E. P. Boden, K. L. Longley, X. Shi, B. L. Lawrence, *Adv. Func. Mat.* **2007**, *17*, 2659–2666.

51 A. Khan, G. D. Stucky, C. J. Hawker, *Adv. Mater.* **2008**, *20*, 3937–3941.

52 V. Cimrova, D. Neher, S. Kostromine, T. Bieringer, *Macromolecules* **1999**, *32*, 8496–8503.

53 A. V. Kolobov, J. Tominaga, *J. Optoelectron. Adv. Mater.* **2002**, *4*, 679–686.

54 A. Zakery, S. R. Elliott, *J. Non-Cryst. Solids.* **2003**, *330*, 1–12.

55 J. Teteris, *Curr. Opin. Solid State Mater. Sci.* **2003**, *7*, 127–134.

56 B. J. Chang, *Opt. Eng.* **1980**, *19*, 642–648.

57 J. M. Kim, B. S. Choi, S. I. Kim, J. M. Kim, H. I. Bjelkhagen, N. J. Phillips, *Appl. Opt.* **2001**, *40*, 622–632.

58 G. J. Steckman, I. Solomatine, G. Zhou, D. Psaltis, *Opt. Lett.* **1998**, *23*, 1310–1312.

59 Y. Gritsai, L. M. Goldenberg, J. Stumpe, *J. Opt.* **2010**, *12*, 015107.

60 G. J. Steckman, V. Shelkovnikov, V. Berezhnaya, T. Gerasimova, I. Solomatine, D. Psaltis, *Opt. Lett.* **2000**, *25*, 607–609.

61 B. M. Monroe, W. K. Smothers, D. E. Keys, R. R. Krebs, D. J. Mickish, A. F. Harrington, S. R. Schicke, M. K. Armstrong, D. M. Chan, C. I. Weathers, *J. Imaging Sci.* **1991**, *35*, 19–25.

62 R. T. Ingwall, M. Troll, *Opt. Eng.* **1989**, *28*, 586–591.

63 R. T. Ingwall, A. Stuck, W. T. Vetterling, OE/LASE'86 Symp (January 1986, Los Angeles), International Society for Optics and Photonics; Proc. SPIE 0615, Practical Holography, pp. 81–87 (August 20, 1986, Los Angeles, CA) 1986, pp 81-87.

64 H. Berneth, F. K. Bruder, T. Fäcke, R. Hagen, D. Hönel, D. Jurbergs, T. Rölle, M. S. Weiser, *Proc. SPIE.* **2011**, 79570H1-79570H15.

65 M. Ayres, K. Anderson, F. Askham, B. Sissom, *SPIE Opt. Eng. Appl.* **2014**, 92010V1–92010V7.

66 M. G. Schnoes, L. Dhar, M. L. Schilling, S. S. Patel, P. Wiltzius, *Opt. Lett.* **1999**, *24*, 658–660.

67 M. L. Calvo, P. Cheben, *J. Opt. A: Pure Appl. Opt.* **2009**, *11*, 024009.

68 N. S. Allen, *J. Photochem. Photobiol. A* **1996**, *100*, 101–107.

69 V. Castelvetro, M. Molesti, P. Rolla, *Macromol. Chem. Phys.* **2002**, *203*, 1486–1496.

70 K. J. Schafer, J. M. Hales, M. Balu, K. D. Belfield, E. W. van Stryland, D. J. Hagan, *J. Photochem. Photobiol. A* **2004**, *162*, 497–502.

71 M. P. Joshi, H. E. Pudavar, J. Swiatkiewicz, P. N. Prasad, A. Reianhardt, *Appl. Phys. Lett.* **1999**, *74*, 170–172.

72 L. Dhar, A. Hale, H. E. Katz, M. L. Schilling, M. E. Schnoes, *Opt. Lett.* **1999**, *24*, 487–489.

73 A. Khan, A. E. Daugaard, A. Bayles, S. Koga, Y. Miki, K. Sato, J. Enda, S. Hvilsted, G. D. Stucky, C. J. Hawker, *Chem. Commun.* **2009**, *4*, 425–427.

74 M. C. Cole, F. R. Askham, W. L. Wilson, U. S. Patent 13,365,304, February 3, **2012**.

75 M. Cole, M. Ayres, U.S. Patent 11,333,527, January 18, **2006**.

76 D. A. Waldman, H. Li, M. G. Horner, *J. Imaging Sci. Tech.* **1997**, *41*, 497–514.

77 K. J. Choi, W. M. Chon, M. Gu, N. Malic, R. A. Evans, *Adv. Func. Mat.* **2009**, *19*, 3560–3566.

78 D. H. Close, A. D. Jacobson, J. D. Margerum, R. G. Brault, F. J. McClung, *Appl. Phys. Lett.* **1969**, *14*, 159–160.

79 R. H. Wopschall, T. R. Pampalone, *Appl. Opt.* **1972**, *11*, 2096–2097.

80 A. Bloom, R. A. Bartolini, D. L. Ross, *Appl. Phys. Lett.* **2003**, *24*, 612–614.

81 W. J. Tomlinson, I. P. Kaminow, E. A. Chandross, R. L. Fork, W. T. Silfvast, *Appl. Phys. Lett.* **1970**, *16*, 486–489.

82 J. M. Moran, I. P. Kaminow, *Appl. Opt.* **1973**, *12*, 1964–1970.

83 M. J. Bowden, E. A. Chandross, I. P. Kaminow, *Appl. Opt.* **1974**, *13*, 112–117.

84 W. J. Tomlinson, E. A. Chandross, H. P. Weber, G. D. Aumiller, *Appl. Opt.* **1976**, *15*, 534–541.

85 M. L. Schilling, V. L. Colvin, L. Dhar, A. L. Harris, F. C. Schilling, H. E. Katz, T. Wysocki, A. Hale, L. L. Blyler, C. Boyd, *Chem. Mater.* **1999**, *11*, 247–254.

86 W. K. Smothers, B. M. Monroe, A. M. Weber, D. E. Keys, In OE/LASE'90, International Society for Optics and Photonics, Los Angeles, CA, January 14–19, **1990**; pp 20-29.

87 G. M. Karpov, V. V. Obukhovsky, T. N. Smirnova, V. V. Lemeshko, *Opt. Commun.* **2000**, *174*, 391–404. no. p

88 V. L. Colvin, R. G. Larson, A. L. Harris, M. L. Schilling, *J. Appl. Phys.* **1997**, *81*, 5913–5923.

89 C. R. Kagan, T. D. Harris, A. L. Harris, M. L. Schilling, *J. Chem. Phys.* **1998**, *108*, 6892–6896.

90 H. Kogelnik, *Bell System Tech. J.* **1969**, *48*, 2909–2947.

91 C. Carre, D. J. Lougnot, J. P. Fouassier, *Macromolecules* **1989**, *22*, 791–799.

92 M. R. Gleeson, J. T. Sheridan, *J. Opt. A: Pure Appl. Opt.* **2009**, *11*, 024008.

93 J. T. Sheridan, J. R. Lawrence, *JOSA A* **2000**, *17*, 1108–1114.

94 J. R. Lawrence, F. T. O'Neill, J. T. Sheridan, *JOSA B* **2002**, *19*, 621–629.

95 M. R. Gleeson, J. V. Kelly, C. E. Close, F. T. O'Neill, J. T. Sheridan, *JOSA B.* **2006**, *23*, 2079–2088.

96 M. R. Gleeson, J. V. Kelly, D. Sabol, C. E. Close, S. Liu, J. T. Sheridan, *J. Appl. Phys.* **2007**, *102*, 023108.

97 M. R. Gleeson, D. Sabol, S. Liu, C. E. Close, J. V. Kelly, J. T. Sheridan, *JOSA B* **2008**, *25*, 296–406.

98 J. V. Kelly, F. T. O'Neill, J. T. Sheridan, C. Neipp, S. Gallego, M. Ortuno, *JOSA B* **2005**, *22*, 407–416.

99 S. D. Wu, E. N. Glytsis, *JOSA B* **2003**, *20*, 1177–1188.

100 S. Martin, C. A. Feely, V. Toal, *Appl. Opt.* **1997**, *36*, 5757–5768.

101 T. Babeva, I. Naydenova, D. Mackey, S. Martin, V. Toal, **2010**, *27*, 197–203.

102 S. Gallego, A. Márquez, D. Méndez, C. Neipp, M. Ortuño, A. Beléndez, E. Fernández, I. Pascu, *Appl. Phys. Lett.* **2008**, *92*, 073306.

103 C. E. Close, M. R. Gleeson, J. T. Sheridan, *JOSA B* **2011**, *28*, 658–666.

104 C. E. Close, M. R. Gleeson, D. A. Mooney, J. T. Sheridan, *JOSA B* **2011**, *28*, 842–850.

105 S. Liu, M. R. Gleeson, J. T. Sheridan, *JOSA B.* **2009**, *26*, 528–536.

106 M. R. Gleeson, S. Liu, R. R. McLeod, J. T. Sheridan, *Josa B.* **2009**, *26*, 1746–1754.

107 F.-K. Bruder, F. Deuber, T. Fäcke, R. Hagen, D. Hönel, D. Jurbergs, T. Rölle, M.-S. Weiser, In OPTO, International Society for Optics and Photonics; Proc. SPIE 7619, Practical Holography XXIV: Materials and Applications, p. 76190I (February 10, 2010, San Francisco, CA) **2010**; pp. 76190I-76190I.

108 C. Barner-Kowollik, F. Bennet, M. Schneider-Baumann, D. Voll, T. Rölle, T. Fäcke, M. S. Weiser, F. K. Bruder, *Polym. Chem.* **2010**, *1*, 470–479.

109 T. Todorov, P. Markovski, N. Tomova, V. Dragostinova, K. Stoyanova, *Opt. Quantum Electron* **1984**, *16*, 471–476.

110 G. Zhao, P. Mouroulis, *J. Mod. Opt.* **1994**, *41*, 1929–1939.

111 E. S. Kovalenko, S. N. Sharangovich, T. E. Zelenskaya, In Proceedings of SPIE 2851, Photopolymer Device Physics, Chemistry, and Applications III; Proc. SPIE 2851, Photopolymer Device Physics, Chemistry, and Applications III, pp. 129–136 (September 30, 1996, Denver, CO) **1996**, pp. 129.

112 D. J. Lougnot, P. Jost, L. Lavielle, *Pure Appl. Opt.* **1997**, *6*, 225–245.

113 D. L. Forman, M. C. Cole, R. R. McLeod, *Phys. Chem. Chem. Phys.* **2013**, *15*, 14862–14867.

114 B. A. Kowalski, A. C. Urness, M. E. Baylor, M. C. Cole, W. L. Wilson, R. R. McLeod, *Opt. Mater. Express* **2014**, *4*, 1668–1682.

115 L. Paraschis, Y. Sugiyama, A. Akella, T. Honda, L. Hesselink, In SPIE's International Symposium on Optical Science, Engineering, and Instrumentation; Proc. SPIE 3468, Advanced Optical Memories and Interfaces to Computer Storage, pp. 55–61 (November 5, 1998, San Diego, CA) **1998**.

116 W. Heller, *J. Phys. Chem.* **1965**, *69*, 1123–1129.

117 T. J. Trentler, J. E. Boyd, V. L. Colvin, *Chem. Mater.* **2000**, *12*, 1431–1438.

118 S. Mikoshiba, A. Hirao, R. Hayase, K. Matsumoto, N. Sasao, T. Kamikawa, U.S. Patent 11,824,029, June 29, **2007**.

119 M.-S. Weiser, T. Rölle, F.-K. Bruder, T. Fäcke, D. Hönel, U.S. Patent 12,569,224, Bayer Materialscience Ag, **2009**.

120 H. Peng, D. P. Nair, B. A. Kowalski, W. Xi, T. Gong, C. Wang, M. Cole, N. Cramer, X. Xie, R. R. McLeod, C. N. Bowman, *Macromolecules* **2014**, *47*, 2306–2315.

121 H. Kou, W. Shi, D. J. Lougnot, Y. Lu, H. Ming, *Polym. Adv. Tech.* **2004**, *15*, 508–513.

122 M.-S. Weiser, F.-K. Bruder, T. Rölle, T. Fäcke, D. Hönel, H. Berneth, U.S. Patent 14,350,593, October 11, Bayer Materialscience Ag, **2012**.

123 A. L. Mikaelian, V. A. Barachevsky, In San Diego, 1991 International Society for Optics and Photonics; San Diego, CA, Proc. SPIE 1559, Photopolymer Device Physics, Chemistry, and Applications II, pp. 246-257 (December 1, 1991, San Diego, CA) **1991**.

124 T. N. Smirnova, O. V. Sakhno, In Holography 2000, International Society for Optics and Photonics, **2000**.

125 N. Suzuki, Y. Tomita, *Appl. Opt.* **2004**, *43*, 2125–2129.

126 N. Suzuki, Y. Tomita, K. Ohmori, M. Hidaka, K. Chikama, *Opt. Express* **2006**, *14*, 12712–12719.

127 O. V. Sakhno, L. M. Goldenberg, J. Stumpe, T. N. Smirnova, *Nanotechnology* **2007**, *18*, 105704.

128 Y. Tomita, K. Furushima, K. Ochi, K. Ishizu, A. Tanaka, M. Ozawa, M. Hidaka, K. Chikama, *Appl. Phys. Lett.* **2006**, *88*, 071103.

129 C. Sanchez, M. J. Escuti, C. van Heesch, C. W. Bastiaansen, D. J. Broer, J. Loos, R. Nussbaumer, *Adv. Funct. Mat.* **2005**, *15*, 1623–1629.

130 K. Omura, Y. Tomita, *J. Appl. Phys.* **2010**, *107*, 3107.

131 E. Hata, K. Mitsube, K. Momose, Y. Tomita, *Opt. Mater. Express* **2011**, *1*, 207–222.

132 R. Fujii, J. Guo, J. Klepp, C. Pruner, M. Fally, Y. Tomita, *Opt. Lett.* **2014**, *39*, 3454–3456.

133 J. Guo, R. Fujii, T. Ono, J. Klepp, C. Pruner, M. Fally, Y. Tomita, *Opt. Lett.* **2014**, *39*, 6743–6746.

134 Y. Tomita, T. Nakamura, A. Tago, *Opt. Lett.* **2008**, *33*, 1750–1752.

135 T. Rölle, F.-K. Bruder, T. Fäcke, M.-S. Weiser, D. Hönel, U. S. Patent 13,504,007, November 2, Bayer Materialscience Ag, **2010**.

136 C. C. Bowley, G. P. Crawford, *Appl. Phys. Lett.* **2000**, *76*, 2235–2237.

137 R. L. Sutherland, V. P. Tondiglia, L. V. Natarajan, T. J. Bunning, W. W. Adams, *Appl. Phys. Lett.* **1994**, *64*, 1074–1076.

138 M. Ortuño, S. Gallego, C. García, C. Neipp, A. Beléndez, I. Pascual, *Appl. Phys. B.* **2003**, *76*, 851–857.

139 T. Mikulchyk, S. Toal, I. Naydenova, *J. Opt.* **2013**, *15*, 105301.

140 T. Nakamura, J. Nozaki, Y. Tomita, K. Ohmori, M. Hidaka, *J. Opt. A: Pure Appl. Opt.* **2009**, *11*, 024010.

141 H. Berneth, F.-K. Bruder, T. Facke, R. Hagen, D. Honel, T. Rolle, G. Walze, M.-S. Weiser, In Proceeding of SPIE; Proc. SPIE 8776, Holography: Advances and Modern Trends III, p. 877603 (May 8, 2013, Prague, Czech Republic) **2013**.